Heterogeneity in Desiccated Solutions: Implications for Biostabilization

Vishard Ragoonanan and Alptekin Aksan
Biostabilization Laboratory, Department of Mechanical Engineering, University of Minnesota, Minneapolis, Minnesota

ABSTRACT Biopreservation processes such as freezing and drying inherently introduce heterogeneity. We focused on exploring the mechanisms responsible for heterogeneity in isothermal, diffusively dried biopreservation solutions that contain a model protein. The biopreservation solutions used contained trehalose (a sugar known for its stabilization effect) and salts (LiCl, NaCl, $MgCl_2$, and $CaCl_2$). Performing Fourier transform infrared spectroscopy analysis on the desiccated droplets, spatial distributions of the components within the dried droplet, as well as their specific interactions, were investigated. It was established that the formation of multiple thermodynamic states was induced by the spatial variations in the cosolute concentration gradients, directly affecting the final structure of the preserved protein. The spatial distribution gradients were formed by two competing flows that formed within the drying droplet: a dominant peripheral flow, induced by contact line pinning, and the Marangoni flow, induced by surface tension gradients. It was found that the changes in cosolute concentrations and drying conditions affected the spatial heterogeneity and stability of the product. It was also found that trehalose and salts had a synergistic stabilizing effect on the protein structure, which originated from destructuring of the vicinal water, which in turn mediated the interactions of trehalose with the protein. This interaction was observed by the change in the glycosidic CO, and the CH stretch vibrations of the trehalose molecule.

INTRODUCTION

Heterogeneity and phase separation

Protein stabilization aims at preserving the native structure of a protein during processing and storage by minimizing (and if possible, completely eliminating) its conformational transitions. This is essential, since the structure of the stabilized protein is directly correlated to its poststorage function and activity (1). During any stabilization process, the thermodynamic state of the medium surrounding the protein is altered (by desiccation, cooling, freezing, or freeze-drying). Since its motions, and therefore its structure, are governed by its surroundings (2), the protein is directly affected by these changes (mostly negatively, by losing its native structure and denaturing). To preserve protein structure, typically, cosolutes (such as salts, sugars, or polyols) are added to the medium as stabilizers (3–5). These stabilizers help alter the chemical and physical properties, and the thermodynamic state of the medium in favor of the protein. Their efficiency is, however, constrained by the thermodynamic, and the kinetic factors associated with the particular stabilization process applied. To achieve successful stabilization of the protein, it is crucial to reach the optimum thermodynamic state ''uniformly'' throughout the medium. If the medium is heterogeneous (i.e., if there are multiple separated phases present that are not in thermodynamic equilibrium with one another), it will continue to evolve during storage, causing degradation of the protein.

Stabilization processes, based on desiccation, cooling, or freezing, are surface-induced and thus are inevitably governed by scale-dependent kinetic constraints. During processing, these kinetic constraints induce heterogeneity (solute and solvent concentration gradients, thermal gradients, and eventually phase separation in the medium). During freezing, ice crystallization induces thermal (due to latent heat release), and concentration gradients (due to solute rejection), causing phase separation in the medium (i.e., formation of regions at different thermodynamic states). For example, during a typical cryopreservation application, initially the bulk water freezes, increasing the concentration of the solutes in the rest of the unfrozen solution. Upon further cooling, the freeze-concentrated solution vitrifies (6). This process creates two distinct regions within the same medium with two distinct states (a metastable phase: glass; and a stable phase: crystalline ice). Presence of different cryopreservation agents such as polyethylene glycol, glycerol, dimethylsulfoxide, sucrose, trehalose, and salts in the medium yield to even more complex thermodynamic and kinetic transitions (7–9), forming multiple thermodynamically distinct regions. Region boundaries have higher free energy to initiate protein denaturation (10), aggregation, and crystallization, and induce discontinuity in the stress field, causing cracking (11). These preservation agents can also interact with the protein through water replacement and preferential exclusion mechanisms. On the other hand, during desiccation of preservation solutions, the solvent is removed by reducing its concentration at the air-liquid interface (for example, by diffusive or convective evaporation of water from the aqueous solution). This creates steep solute concentration and temperature gradients within the solution, yielding to solute aggregation, skin formation, crystallization, and cracking within the desiccated medium (12).

Submitted April 12, 2007, and accepted for publication October 24, 2007.

Address reprint requests to Alptekin Aksan, E-mail: aaksan@me.umn.edu.

Editor: Jane Clarke.

0006-3495/08/03/2212/16 $2.00

doi: 10.1529/biophysj.107.110684

Heterogeneity is unavoidable even during rapid desiccation of very thin films of biopreservation solutions (13).

Phase separation during desiccation, freezing (9), and lyophilization (14) processes has been previously observed and quantified in bulk solutions, mainly by thermal, kinetic, and calorimetric analyses of biopreservation solutions (15–18), and solutions containing proteins (19–21). The ultrastructure of the processed products was visualized by scanning electron microscopy (22,23), and analyzed by infrared (IR) imaging (21) and spectroscopy of the bulk product (24). However, to date, irrespective of the stabilization process applied, it has not yet been reported how the protein populations are distributed among different thermodynamic regions within the same product, and what role(s) the population distribution plays in determining the stabilization efficacy of the biopreservation solution or the process, and the postthaw activity of the bulk product.

Desiccation phenomena

For desiccated state preservation of proteins (or any biomaterial and organism), currently available methods are freeze-drying (lyophilization) (25,26), foam vitrification, spray-drying (27,28), and isothermal diffusive/convective drying (29,30). Depending on the application, all of these methods have major advantages that make them particularly more efficient under certain conditions. For example, one advantage of isothermal drying, with respect to lyophilization (especially at commercial production scales), is that the process does not require specialized cryogenic and low-pressure equipment or process, thus reducing processing costs.

Desiccation processes are of interest not only in preservation research, but also in deposition of thin films, surface patterning (31), bioreactive and biosensing coatings (32), ink-jet printing (33), microarray analysis of biomolecules (34,35), and more recently in the early diagnosis of disease in bodily fluids (36), detection of very low concentrations of chemicals and contaminants in solutions (37,38), and separation of nanoparticles from solutions (39,40).

Desiccation kinetics of a solution drying in contact with a surface is mainly affected by the environmental conditions (such as temperature and relative humidity (RH)), the chemical composition of the solution, and the interactions of the solution with the surface it is dried on. Environmental conditions act on the surface of the solution, mainly affecting the evaporation rate of the solvent. Chemical composition of the solution determines its physical, chemical, and rheological properties, the diffusivity of the solvent (and the cosolutes) in the solution, crystallization rates of the cosolutes, and ultimately, the final thermodynamic state after drying. Hydrophilic surfaces induce contact line pinning for sessile droplets, causing ring-like deposits in the periphery (41,42). One of the main factors contributing to spatial heterogeneity in a drying sessile droplet is the variation of the solvent evaporation flux on the droplet surface. The evaporation flux is lowest at the center of the droplet but increases toward the pinned periphery (Fig. 1). This is associated with the higher probability of escape for the solvent molecules located at the periphery of the droplet (41). Higher evaporation flux at the droplet periphery induces a radially outward flow (Fig. 1) within the desiccating droplet (called the peripheral flow) (41). The peripheral flow continues as long as the driving force (i.e., the evaporation flux at the surface) is higher than the opposing force (the viscous drag on the solute particles). This flow is opposed (43) or sometimes even strengthened (44) by the Marangoni flow fueled by the temperature and solute concentration dependence of the surface tension (45). Due to nonuniform evaporation flux on the sessile droplet surface, the temperature at the surface is lowest at the periphery and highest at the center. Due to peripheral flow, on the other hand, the solute concentration is higher at the periphery. These two factors interact to create Marangoni instability. In some cases, recirculation zones appear within the drying droplet due to the synergistic effects of the Marangoni flow with the peripheral flow (43,46). In other cases, the Marangoni flow may weaken the effects of the peripheral flow by carrying the solutes back to the center of the droplet.

Specific interactions

Another factor that is of importance is the specific interactions among the constituents (cosolutes and the protein) in the solution. With increased crowding within the desiccating droplet, these interactions become more significant. Most biopreservation solutions incorporate cosolutes such as the nonreducing sugar, trehalose (47). Trehalose has been shown to be beneficial in stabilizing biomaterials and organisms during freezing, drying, lyophilization, and storage (5,48,49). Presence of other solutes such as cations and anions in the biopreservation solution can enhance stability (50,51) through an unknown synergistic effect (52,53). The interactions between ions and carbohydrates have been observed in the form of cation-carbohydrate complexes (54,55), and the change in the physical and thermodynamic properties of concentrated trehalose solutions by anions (56). For example, Mazzobre et al. (52) documented an increase in the stability of β-galactosidase upon drying in the presence of trehalose and Mg^{2+} (which they attributed to delayed crystallization of

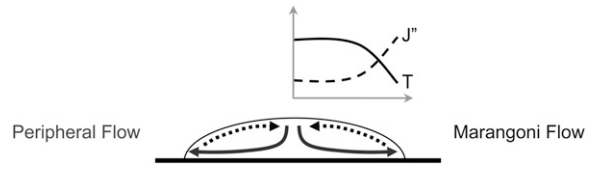

FIGURE 1 Schematic of a drying sessile droplet. (*Solid line*) peripheral flow, (*dashed line*) Marangoni flow. The graph represents the variation of temperature (T) and the solvent evaporation flux (J'') on the surface of the droplet.

trehalose). Since it is hypothesized that the mechanism of stabilization by all cosolutes is through ordering, structuring, and changing the thermodynamic phase or state of the water around biological materials (by water replacement (27) and preferential exclusion mechanisms (57)), it is possible that ions also affect the hydration characteristic of sugars and the proteins.

All of these physical, rheological, kinetic, and chemical factors described above, when combined, create quite an unpredictable outcome even for a seemingly simple process as sessile droplet desiccation. Fig. 2 shows images of $V_i = 1.0\ \mu l$ (V_i: initial volume) desiccated droplets (dried on BaF_2 windows for 24 h at room temperature and 0% RH) that contain a model protein (lysozyme), a sugar (trehalose), and various salts. Visually, significant differences are observed among different samples; even spatial variations are seen within the same sample. This brings up questions of what these visual differences mean in terms of the microstructure, the distribution of solutes within the droplet, and the structure of the protein. These questions become of paramount interest since traditionally, in biopreservation research, proteins, cells, and bacteria are suspended in biopreservation solutions, which are then deposited on a surface (usually in the form of a thin film or droplet), where they are convectively or diffusively dried under controlled conditions (29,58,59). Upon rehydration, the activity or the viability of the whole population is measured (without any regard for the heterogeneity within the dried droplet).

We hypothesize that due to the factors examined above, different populations of the biological materials and organisms experience very significantly different histories and microenvironmental conditions during processing and storage. This is reflected in the heterogeneity of the medium, which affects the poststorage activity. We further hypothesize that this directly affects the outcome of the experiments performed to determine the preservation efficiency of a particular cosolute, preservation solution, or the preservation technique. To test these hypotheses, in this research we focused on:

1. Quantifying the spatial heterogeneity in desiccated sessile droplets in terms of the solute (trehalose, salt, and lysozyme) and water concentration gradients, phase-separation tendencies, and the thermodynamic states of the coexisting separated phases.
2. Exploring the effects of the local variations of trehalose, salt, and lysozyme concentrations on the thermodynamic phases and states of the desiccated solution.
3. Establishing the interactions of salts and trehalose in stabilizing the secondary structure of the desiccated lysozyme.

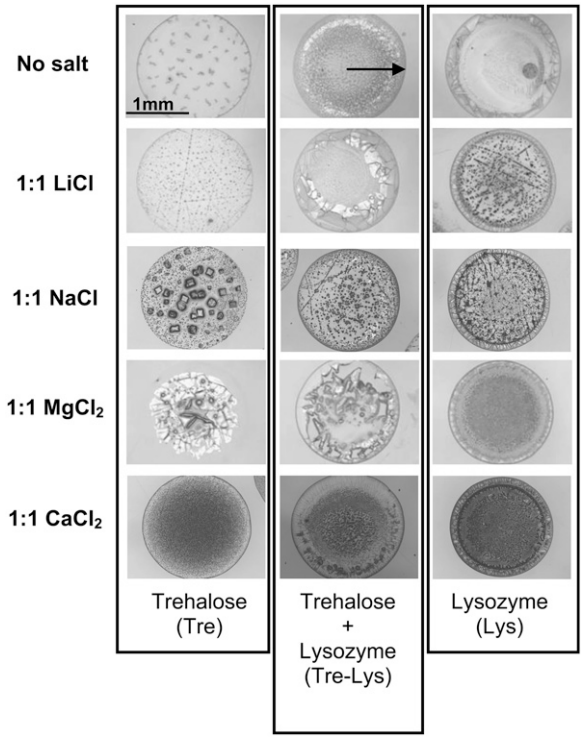

FIGURE 2 Photomicrographs of aqueous sessile droplets ($V_i = 1.0\ \mu l$) dried on BaF_2 windows at room temperature and 0% RH for 24 h. Each row corresponds to a different salt present in the solution at a 1:1 molar ratio to trehalose.

MATERIALS AND METHODS

High purity trehalose dihydrate was purchased from Pfanstiehl (Ferro Pfanstiehl Laboratories, Waukegan, IL). Other chemicals (LiCl, NaCl, $CaCl_2.2H_2O$, $MgCl_2.6H_2O$) and the model protein (hen egg white lysozyme) were purchased from Sigma (St. Louis, MO). All of the solutions were prepared gravimetrically on a microbalance using ultrapure water. Ultrapure water (with electrical resistivity >18.2 MΩ·cm at 25°C) was obtained using a Milli-Q water purification system (Millipore, Billerica, MA) through filtering of deionized water. Experimental solutions were prepared using combinations of 1, 2.5, or 5% w/w trehalose (TRE), 0.5% w/w lysozyme (LYS) and 1:1 molar ratio of salt to TRE. The four different salts used in this study were LiCl, NaCl, $MgCl_2$, and $CaCl_2$. The mass of water in the hydrates was accounted for in measuring the required mass of water to prepare the solutions. The initial concentration of TRE in the solution (1% w/w) was chosen to minimize desiccation-induced instabilities in the drying biopreservation solution based on previous experience (12). The ratio of TRE to LYS was chosen based on previous results of Carpenter et al. (49) showing the effectiveness of TRE in stabilizing freeze-dried LYS at that specific ratio. In the samples containing LYS and salt (LYS-salt), the salt content was the same as the solutions containing trehalose, lysozyme, and salt (TRE-LYS-salt). Before experiments, the solutions were mixed vigorously and passed though a Teflon filter (0.2 μm pore size). $V_i = 1.0$ or 10 μl of the experimental solutions were deposited on BaF_2 windows and dried at 22°C and 0% RH in sealed drying boxes containing excess amounts of $CaSO_4$. BaF_2 windows were used as they provided a hydrophilic surface in addition to being transparent in the infrared light region of interest. After desiccation for 24 h, the BaF_2 windows containing the samples were transferred to an IR microscope connected to a Fourier transform infrared spectroscope (FTIR: Thermo-Nicollet 6700 equipped with a deuterated triglycine sulfate detector; Thermo Electron, Waltham, MA). FTIR spectra (in the range of 930 to 4000 cm^{-1}) were recorded using an aperture size corresponding to an area of $100 \times 100\ \mu m$ on the sample. On each sample, multiple IR spectra were collected, starting from the center of the droplet and moving in a radially

outward direction in 100 μm increments. A total of 64 IR scans were collected and averaged at each location. Similar drying experiments were carried out to establish the effects of hydrophobic surfaces (such as gold-coated microslides or CaF_2 windows) on the desiccation kinetics of droplets, the final state and the uniformity of LYS concentration in the desiccated droplet. Photomicrographs of the desiccated droplets were taken by a digital camera attached to the IR microscope.

Data analysis

Distribution of TRE within the dried solutions was determined using the absorbance intensity of the 1150 cm^{-1} band corresponding to the ν-CO of the glycosidic bond. Distribution of LYS was determined using the absorbance intensity of the amide-II band located at ~1540 cm^{-1}. Desiccation-induced changes in LYS secondary structure were observed by the changes in the amide-I (1600–1700 cm^{-1}) and amide-II (1510–1580 cm^{-1}) bands. In addition to incorporating bands attributed to backbone conformations of proteins, amide-I band also involves contributions from a water-bending mode, making protein analysis difficult. Amide-II band (associated with δ-NH and ν-CN in protein side groups), on the other hand, is not affected by spectral contributions from water. Upon desiccation of the protein, the amide II band broadens due to an increase in the absorption at the frequency corresponding to β-sheet structures located at 1535 cm^{-1} (60). To quantify the resultant changes in the protein structure, a correlation coefficient, r, which is based on the shape of the amide II band, was utilized. The correlation coefficient, r, is given by (1)

$$r = \frac{\sum x_i y_i}{\sqrt{\sum x_i^2 \sum y_i^2}}, \quad (1)$$

where x_i and y_i represent the spectral absorbance values of the second-derivative spectra at the ith wavenumber position for the reference (i.e., fully hydrated LYS), and the desiccated protein, respectively, in the region 1510–1550 cm^{-1}. $r = 1.0$ indicates that the protein preserved its native secondary structure, and $r \rightarrow 0$ that its secondary structure changed (i.e., the protein denatured).

RESULTS

Experiments were performed to quantify heterogeneity in desiccated sessile droplets of a biopreservation solution containing TRE and salt, and LYS. The changes in the secondary structure of the lysozyme were analyzed to probe the solute-protein interactions in different regions of the droplet.

Salt solutions

To establish a baseline for measurements, experiments were performed with sessile droplets containing aqueous salt solutions ($V_i = 1$ μl), which were deposited on BaF_2 windows and dried extensively (24 h at room temperature and 0% RH). Desiccated droplets that contained LiCl, $MgCl_2$, and $CaCl_2$ produced IR spectra with double peaks in the amide-I region, typical for hydrated crystalline structures (61). In these droplets, the water combination peak located at 2150 cm^{-1} also changed in shape and location, showing strong water-salt interactions. On the other hand, dried droplets that contained NaCl did not exhibit water-related spectral features. This is expected since NaCl does not form crystalline hydrates at room temperature and ambient pressure (62). These experiments showed that even with extensive drying at room temperature, water could remain entrapped in salt crystals.

TRE, LYS, and LYS-TRE solutions

In TRE solutions, spectral peaks in the TRE fingerprint region (900–1200 cm^{-1}) shifted to lower wavenumbers upon drying, indicating a decrease in hydrogen bonding in TRE. This was also confirmed by the measured decrease in the magnitude of the 1047 cm^{-1}, peak indicative of a decrease in the hydrogen bonding of the COH groups (63). TRE mainly accumulated at the periphery of the desiccated droplet (mainly within 300 μm of the droplet edge) in the form of a ring (Fig. 3 *a*). This was due to a rather strong peripheral flow within the droplet, typical for desiccating droplets experiencing contact line pinning (41). The amount of water entrapped in the TRE droplet also varied spatially and was largest at the periphery of the droplet, where TRE accumulation climaxed. There was no evidence of crystallization of TRE. Rather, in accord with previously published results, TRE remained amorphous (12).

In LYS solutions, LYS mainly accumulated in the outer periphery (70% of the total population) in a narrower ring confined to 100–150 μm from the edge of the dried droplet (Fig. 3 *b*) following a very steep concentration gradient. Throughout the sample, the shape and the location of the amide-II peak was significantly different from that in the native state (Fig. 4 *a*) with $r_{average} = 0.68$. The spatial variation of r was independent of the local concentration of LYS. In the dried LYS droplets, there was a dark spot located in the center region, which had a higher LYS concentration than the surrounding area (Fig. 2). Exact location of the dark spot varied from experiment to experiment, but it was always in the center region. The formation of the dark spot was attributed to a weak Marangoni flow (43), which carried the protein to its locus. r values measured in the dark spots were not different from those in the surrounding areas.

In the LYS-TRE solutions, the final spatial distribution of LYS was altered due to the presence of TRE. The LYS concentration gradient in the outer periphery was less steep, which caused an increase in the width of the deposition ring to 400–450 μm (Fig. 3 *c*). This was attributed to the higher viscosity of the solution, which decreased the speed and duration of the peripheral flow. The spatial distribution of TRE in the LYS-TRE solution also varied from that in the TRE only solution. The most significant difference was in the outer periphery, where the TRE concentration decreased with respect to the peripheral region due to a very high concentration of LYS in this region (probably due to high surface affinity of LYS). This caused a very significant drop in the TRE/LYS ratio at the outer periphery (at ~700 μm). There was no evidence of a Marangoni flow in the droplet. In

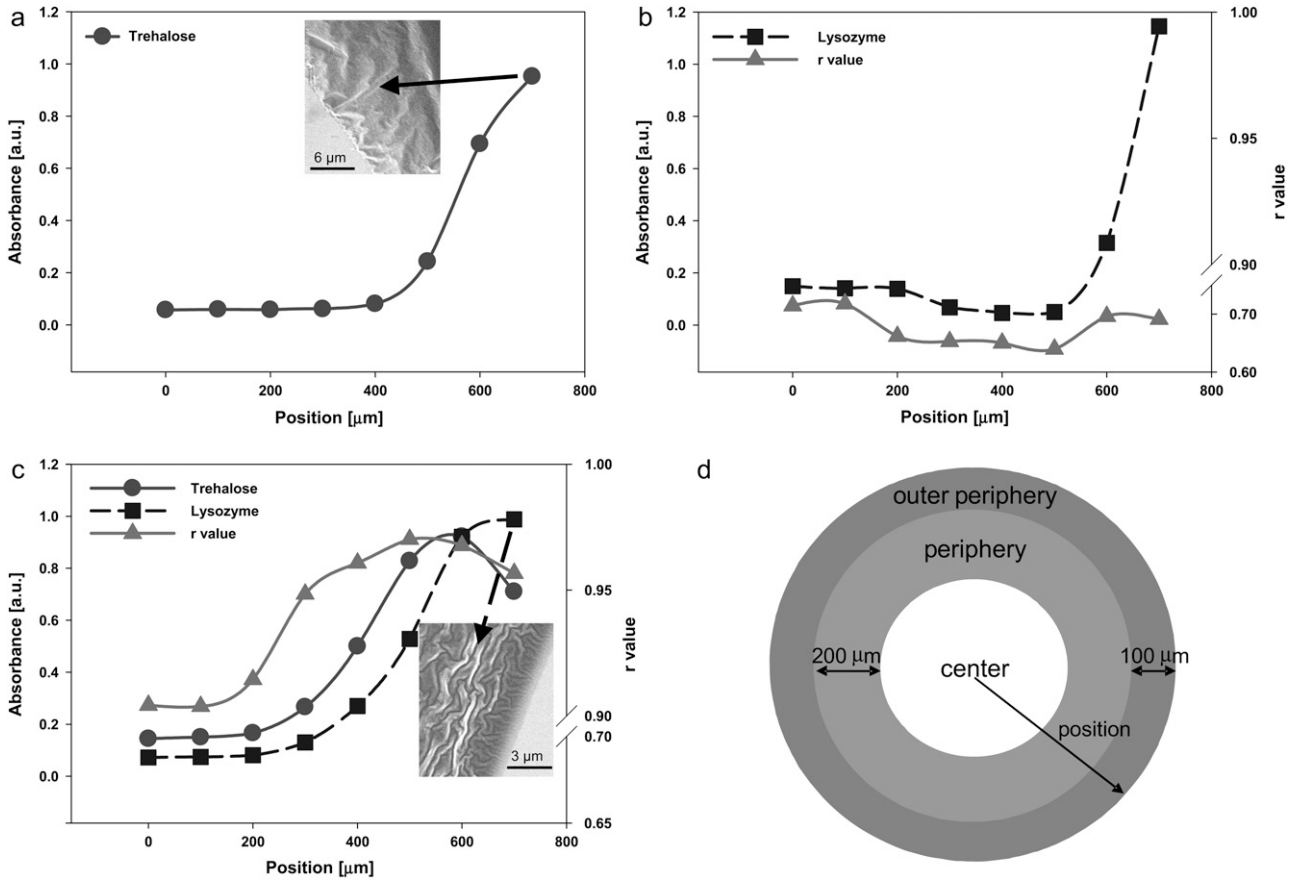

FIGURE 3 (*a*) Dried TRE solution (*inset*, SEM image of the outer periphery region), (*b*) dried LYS solution, (*c*) dried LYS-TRE solution (*inset*, SEM image of the outer periphery region), and (*d*) the locations of the outer periphery, periphery and the center of the dried droplet. *X* axis (position) in the figure corresponds to the radial distance from the center of the droplet.

the presence of TRE, *r* values for LYS increased significantly, ranging from 0.9 to 0.97 ($r_{\text{average}} = 0.94$) throughout the sample (Table 1). The most significant increase was in the periphery, where the TRE concentration peaked. Even though the TRE concentration was lower in the center (when compared to the periphery), *r* values were still higher ($r_{\text{center}} = 0.9$) than LYS-only samples ($r_{\text{average}} = 0.68$).

These results clearly showed the spatial variations of TRE and LYS concentrations in the desiccated droplets, mainly caused by a peripheral flow and the high surface affinity of LYS. Various regions in the desiccated droplet are defined in Fig. 3 *d*. IR spectra in the amide-I and amide-II range obtained from different solutions are presented in Fig. 4, *a* and *b*. Note the difference in the amide-II region between the hydrated and dried LYS, and the similarity between the hydrated LYS and the LYS-TRE solutions.

TABLE 1 Effect of salts on protein secondary structure

Sample	r_{average} (Range)	Sample	r_{average} (Range)
LYS	0.69 (0.69–0.76)	LYS-TRE	0.94 (0.90–0.97)
LYS-LiCl	0.68 (0.5–0.8)	LYS-TRE-LiCl	0.99 (0.95–0.99)
LYS-NaCl	0.75 (0.6–0.8)	LYS-TRE- NaCl	0.95 (0.92–0.99)
LYS-$MgCl_2$	0.9 (0.6–0.92)	LYS-TRE- $MgCl_2$	0.97 (0.91–0.99)
LYS-$CaCl_2$	0.82 (0.45–0.9)	LYS-TRE- $CaCl_2$	0.95 (0.94–0.97)

Salt solutions with LYS

Desiccated LYS-salt solutions (containing 0.5% w/w LYS and a 1:1 molar ratio of LYS/salt) exhibited similar LYS concentration distributions as the LYS solutions, with >60% of the LYS population accumulating in the outer periphery. The width of the ring structure was ~100–150 μm, similar to that in LYS solution, showing the negligible effect of the added salts in increasing the viscosity of the solution and slowing the peripheral flow.

In the LYS-salt solutions, probably due to being excluded from the protein rich periphery, salts crystallized primarily in the central region (Fig. 2). Since salts did not have distinct IR fingerprint spectra, it was not possible to detect their accumulation in the periphery. However, no salt crystals were visually observed in the periphery. This meant that even if salts were also present in the periphery, they did not form

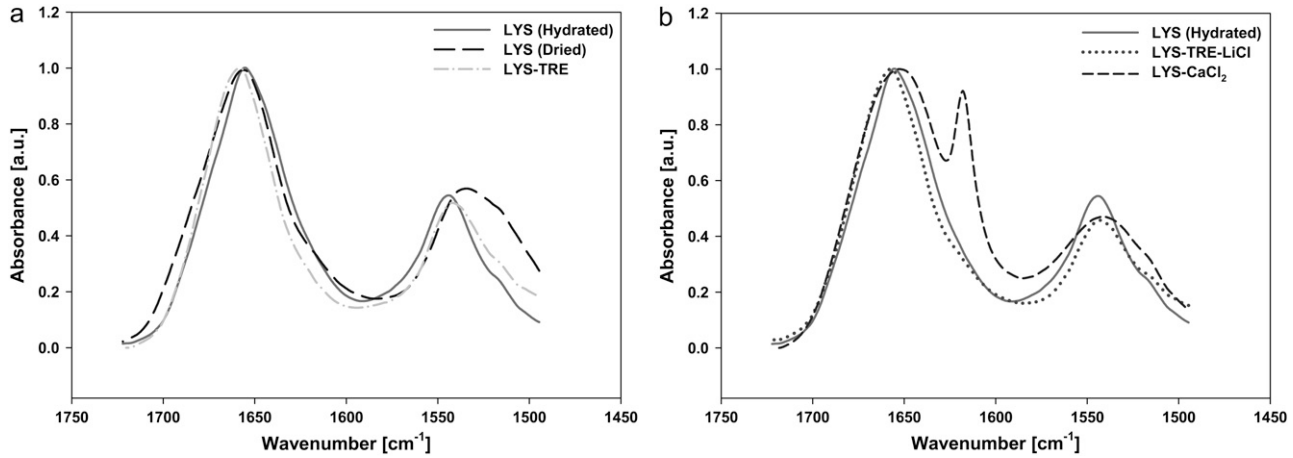

FIGURE 4 IR spectra of the Amide I and Amide II bands of (*a*) hydrated LYS ($r_{center} = 1$), dried LYS ($r_{center} = 0.65$), and dried LYS-TRE ($r_{center} = 0.93$), (*b*) Hydrated LYS ($r_{center} = 1$), dried LYS-TRE-LiCl ($r_{center} = 0.99$), and dried LYS-$CaCl_2$ ($r_{center} = 0.77$).

crystals of any composition (i.e., salt-salt or salt-protein). LYS-salt droplets did not display the dark spots observed in the LYS samples. These observations indicated that even at low concentrations, salts weakened the concentration and the temperature dependence of the surface tension, therefore stopping the Marangoni flow.

LYS-$MgCl_2$ and LYS-LiCl samples contained spectral features similar to those of their respective crystalline hydrates. For an extensively dried LYS-LiCl sample, there was an increase in the absorbance of the peak corresponding to the carboxylate group in the hydrated protein (64) located at 1580 cm^{-1}. This could be attributed to the interaction of LiCl with the COO^- groups of LYS, similar to what is observed with Ca^{2+} ions and equine lysozyme (65). Spectra from LYS-NaCl samples were identical to that from LYS samples, indicating that NaCl had little, if any, direct interaction with the LYS upon drying, even though its presence in the solution stopped the Marangoni flow. The structure of LYS in the LYS-$CaCl_2$ sample (Fig. 4 *b*) was quite different from that of the hydrated LYS (and also different from those in other LYS-salt samples). There was a significant broadening of the amide-I peak (a change typical of the formation of β-sheet structures in proteins (66)) as compared to other dried samples, and the formation of an adjacent peak showing the presence of crystalline hydrate structures. These data also show that, as opposed to other salts, $CaCl_2$ preferentially interacted with LYS upon drying. This was also shown by Arakawa et al. (50) by measuring the change in the partial specific volume of the protein in the presence of salts. Arakawa et al. concluded that the observed effect was primarily due to the Ca^{2+} ion binding to the protein (but not the Cl^- ion). Mizughchi (65) also observed the an interaction between equine lysozyme and the Ca^{2+} ion.

In summary, spatially averaged r values in the desiccated droplets were $r_{LYS\text{-}LiCl} \leq r_{LYS}$, $r_{LYS\text{-}NaCl} < r_{LYS\text{-}CaCl2} \leq r_{LYS\text{-}MgCl2}$ (see Table 1 for details). Overall, average r values were significantly higher for LYS-$CaCl_2$ and LYS-$MgCl_2$, probably due to specific salt-protein binding interactions, which is not within the scope of the research presented here.

Salt solutions with TRE

TRE-salt solutions had similar TRE distribution as in the TRE solutions, with TRE mainly accumulating at the periphery of the droplet. In the presence of salts, there was an increase in the absorbance of the TRE δ-CH band located at 1420 cm^{-1}, whereas the asymmetric ν-CH peak (originally located at 2930 cm^{-1} for the dried TRE, and at 2943 cm^{-1} for TRE in solution) shifted to higher wavenumbers as compared to the dried TRE sample. TRE-$MgCl_2$ samples had the greatest shift in the ν-CH peak (new location was at 2945 cm^{-1}, even higher than TRE in solution), followed by LiCl (2941 cm^{-1}), NaCl (2938 cm^{-1}), and $CaCl_2$ (2938 cm^{-1}). There was a decrease in the intensity of 1030 cm^{-1} peak in TRE in the presence of salts. This peak is associated with ν-CO, ν-CC, and δ-COH at C-4-O (which was attributed to a change in hydrogen bonding) (63). There was also a shift in the frequency of the glycosidic bond (originally located at ~1150 cm^{-1}) toward lower wavenumbers. This shift was greatest in the presence of $CaCl_2$ and smallest in the samples containing LiCl and $MgCl_2$. TRE and TRE-NaCl samples had similar glycosidic bond frequencies, further proving that NaCl did not significantly affect the remaining water in the vicinity of TRE. The ν-OH peak located at ~3360 cm^{-1} for the dry TRE sample shifted to lower wavenumbers in TRE samples containing LiCl, NaCl, $MgCl_2$, and $CaCl_2$. The lowest wavenumbers for the ν-OH peak were observed for the TRE-LiCl sample. The location of the ν-OH peak gives a measure of hydrogen bonding with lower wavenumbers that is indicative of a higher degree of hydrogen bonding.

TRE-LiCl samples did not exhibit salt hydrate peaks, which indicated that LiCl did not crystallize out in the

presence of TRE upon drying (as opposed to LiCl solutions). As NaCl did not form crystalline hydrates, it was not directly possible to determine if there was any change in the crystallization kinetics of the salt in the presence of TRE. However, the changes in the δ-CH band (1420 cm^{-1}) of TRE showed some interaction of NaCl with TRE. TRE-$MgCl_2$ samples did not exhibit the characteristic crystalline hydrate peaks of $MgCl_2$, but there was evidence of its interaction with the residual water as seen by a shift in δ-HOH to higher wavenumbers. TRE-$MgCl_2$ samples had more entrapped residual water than any other TRE-salt sample. TRE-$CaCl_2$ samples did not have crystalline hydrate peaks for the samples dried on gold-coated or CaF_2 windows, but seemed to interact with TRE as seen from significant changes in all peaks related to the carbohydrate backbone.

Formation of cation-TRE complexes have been reported in the literature (67,68), specifically for $CaCl_2$ (68), which forms a monohydrate complex with TRE. TRE-$CaCl_2$ samples dried on BaF_2 windows had small hydrate-like peaks (Fig. 4 *b*), in addition to the spectral features observed for TRE-$CaCl_2$ samples dried on gold-coated and CaF_2 windows. In these samples, the coexistence of the crystalline peaks, hydrate-like peaks, and peaks typical of amorphous trehalose (69) proved the presence of multiple thermodynamic phases within the same region of the desiccated droplet: amorphous trehalose, $CaCl_2$ crystalline hydrate, and $CaCl_2$-trehalose complexes.

These results showed the strong interaction of salts (especially $CaCl_2$) with the residual water, and TRE at low water activity conditions, commonly reached during desiccated-state preservation, and lyophilization of proteins and organisms.

Salt solutions with LYS-TRE

All LYS-TRE-salt droplets had similar deposition patterns irrespective of the salt, with higher accumulation of LYS toward the outer periphery (Fig. 5), following a steep gradient. The difference in the distribution of TRE with respect to LYS was very significant in all of LYS-TRE-salt droplets (similar to the LYS-TRE case examined before). In LYS-TRE-salt droplets, LYS reached its maximum concentration at the edge of the droplet, whereas TRE reached its maximum concentration at a distance of $\sim 100-200\ \mu$m from the edge, dropping to lower values at the edge. This meant that the two constituents (the protein and the sugar) within the

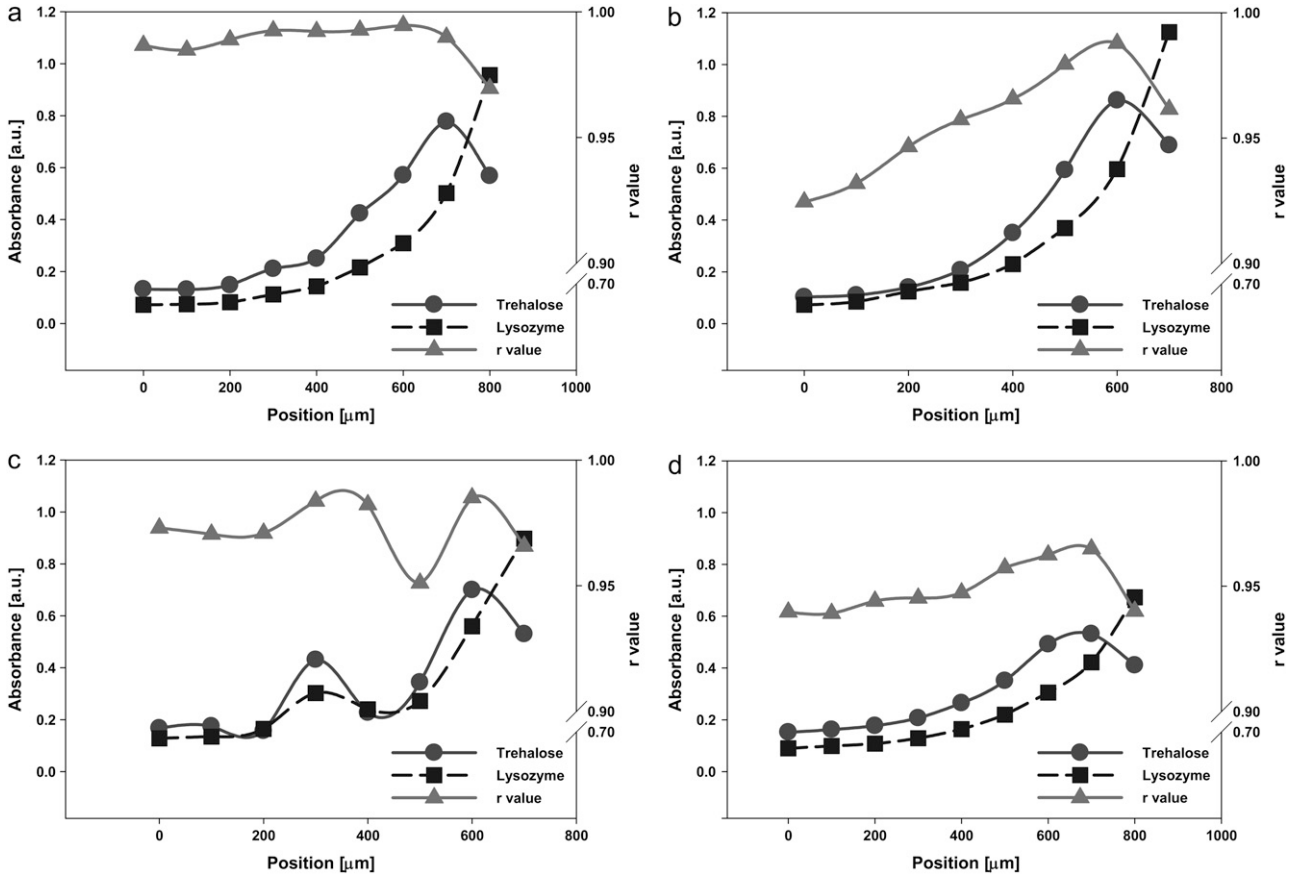

FIGURE 5 Distribution of LYS and TRE and variation of *r* values within the dried (*a*) LYS-TRE-LiCl, (*b*) LYS-TRE-NaCl, (*c*) LYS-TRE-$MgCl_2$, and (*d*) LYS-TRE-$CaCl_2$ droplets. *X* axis (position) in the figure corresponds to the radial distance from the center of the droplet.

solution started to separate during drying. In general, the TRE/LYS ratio did not change with location at the center of LYS-TRE and LYS-TRE-salt solutions, but showed great variation at the outer periphery, where the largest population of LYS had accumulated. In LYS-TRE-salt solutions, even though little or no crystalline or hydrate spectral peaks were observed, there was visual evidence of some salt precipitation toward the center of the droplet. This might be due to higher concentrations of salt accumulating at the center of the droplet, increasing the probability of precipitation. The absence of hydrate peaks in most spectra was due to less salt precipitation as compared to LYS-salt samples similar to what was observed for TRE-salt samples.

Overall, LYS in LYS-TRE-salt samples had a similar secondary structure to the LYS-TRE sample (Table 1). However, the LYS-TRE-LiCl sample had the highest $r_{average}$ value and the smallest variation in r within the droplet (Fig. 5 *a*). Very few crystal structures were observed in the TRE-LYS-LiCl samples. The LYS-TRE-NaCl samples had the greatest variation in r values moving away from the center (Fig. 5 *b*). This might be due to the heterogeneous crystallization of the NaCl at the center of the droplet. TRE-LYS-$MgCl_2$ had variations in protein structure, which were in part related to the nonuniform variation of the TRE/LYS ratio within the droplet (Fig. 5 *c*). Close inspection of the IR spectra revealed that the TRE-LYS-$MgCl_2$ sample had higher water content than any of the other samples, probably affecting the structure of the LYS in a positive way. The presence of high water content was attributed to the high coordination number of the Mg^{2+} cation. No crystal structures were observed visually in the TRE-LYS-$MgCl_2$ samples. TRE-LYS-$CaCl_2$ samples had small variations in r (Fig. 5 *d*) compared to LYS-TRE-NaCl and TRE-LYS-$MgCl_2$. Certain crystalline structures were present away from the periphery, which also corresponded to relatively lower r values. It was observed for all of the LYS-TRE and LYS-TRE-salt samples that the decrease in the TRE/LYS ratio at the outer periphery (where the majority of the LYS population accumulated) caused a decrease in r.

In summary, in all samples $r_{average}$ values ranged between 0.88 and 0.99 (Table 1). The higher r values measured in the TRE-LYS-LiCl sample were probably due to the lower crystallization tendency of LiCl and another synergistic mechanism, which will be further discussed in subsequent sections. It was noted that in the experiment concentrations, LiCl was the ''best'' in terms of maintaining high r values throughout the sample even though it could not completely eliminate the spatial separation of the constituents (LYS and TRE).

All of the results are summarized in Fig. 6, where the size of the symbols represents the percent total population of LYS accumulated in a specific region within the dried droplet: 70% of the total LYS population accumulated at the outer periphery in LYS solutions. This value dropped to 40% in the LYS-TRE samples. In the LYS-TRE-salt samples, the LYS population in the outer periphery ranged from 45 to 55%. The lowest populations were obtained with solutions containing $CaCl_2$, and the highest with NaCl. Mainly, the strength (and probably the duration) of the peripheral flow dictated the size of the LYS population in the outer periphery. With increased solution viscosity, the strength of the flow decreased. In the TRE-$CaCl_2$ solution, viscosity was the highest, and in the TRE-NaCl solution it was the lowest (data not shown).

Changes in the structure of TRE

Spectral features of TRE were similar to those in the dried TRE-salt droplets: There was a shift in the 1150 cm^{-1} band of the glycosidic bond, and a shift in the ν-CH peak to higher wavenumbers as compared to the TRE-LYS sample. These shifts were investigated to elucidate the relation between the TRE and LYS structures. It was observed that an increase in the ν-CH frequency was generally matched with an increase in r (Fig. 7 *a*). r values approached the maximum value of

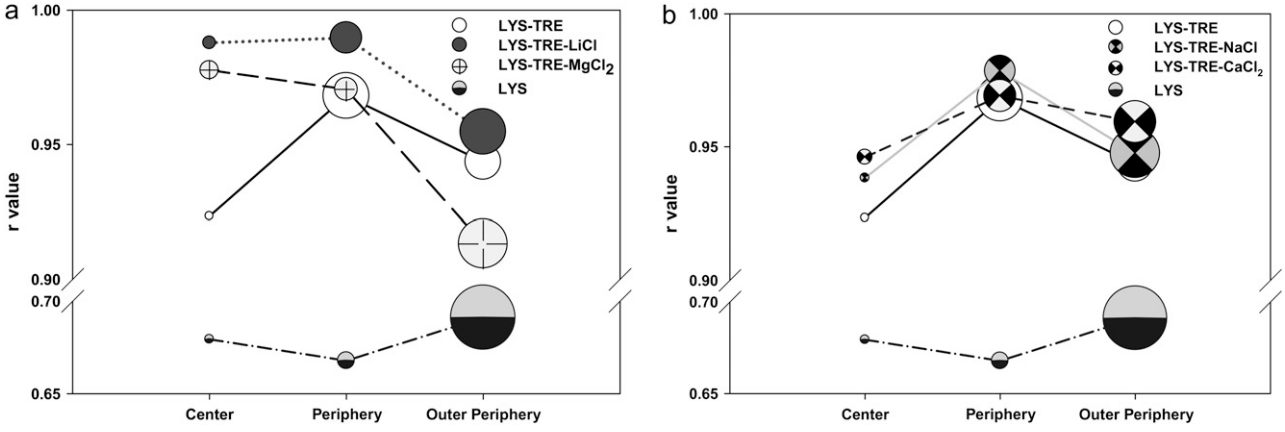

FIGURE 6 Change in r with location within dried droplets. The size of the circles represents the population of LYS at the respective region within the droplet.

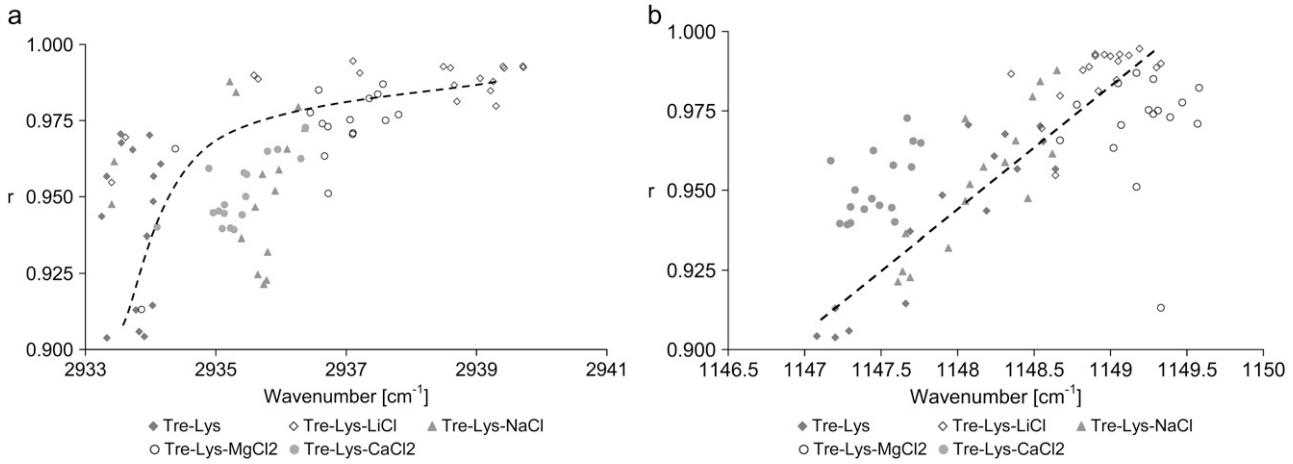

FIGURE 7 Change in lysozyme structure (r) with (a) trehalose glycosidic ν-CO and (b) asymmetric ν-CH peak locations. Dashed lines are guide for the eye.

1.0 (hydrated LYS) as the ν-CH frequency approached that of fully hydrated TRE in solution (2943 cm^{-1}). It was further observed that a higher glycosidic wavenumber correlated well with an increase in r (Fig. 7 b). The general trend also indicated that higher r values were obtained as the glycosidic wavenumber approached that of TRE in solution (1150 cm^{-1}). These results point toward a modification in the hydration characteristics of TRE in the presence of salts and indicate the existence of a relation between the structure of TRE and LYS.

Factors affecting LYS distribution

With increasing TRE to LYS concentration in the initial solution, LYS accumulation patterns changed significantly. At 2.5% w/w TRE concentration (Fig. 8 a), the high viscosity of the solution slowed the peripheral flow significantly, therefore broadening the deposition ring (compare the LYS distribution for 1% w/w TRE in Fig. 3 c). This resulted in a higher accumulation of LYS at the center region of the droplet, with smoother gradients at the periphery. The higher concentration of TRE also decreased the drop in the TRE/LYS ratio at the outer periphery. This enabled a more uniform distribution of r within the droplet, with the $r_{average}$ reaching 0.97. With further increasing the initial TRE concentration to 5% w/w (Fig. 8 b), the effect became much more significant, yielding to a more uniform distribution of LYS and r values ($r_{average} = 0.98$).

The strength of the peripheral flow could also be reduced (without changing the composition of the solution) by forcing the evaporation rate distribution at the surface of the droplet to be more uniform. This was achieved by placing the droplet in a small chamber, which had a small hole drilled right above the center of the droplet. The air outside the chamber was kept at 0% RH and room temperature. In this setup, the evaporation rate on the surface of the droplet reached a maximum at the center (right below the hole) and a minimum at the periphery (far away from the hole), eliminating the driving force behind the peripheral flow (41). This drying condition promoted the formation of a more uniform deposit (both in terms of the TRE and LYS

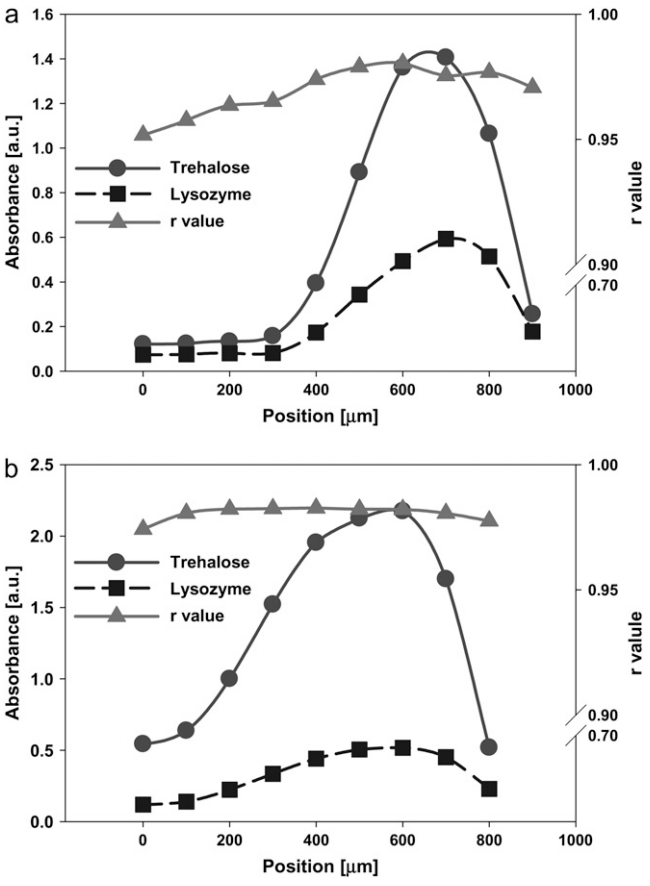

FIGURE 8 Distribution of LYS and TRE and variation of r values within dried (a) LYS-TRE (2.5% TRE) and (b) LYS-TRE (5% TRE) droplets. Xx axis (position) in the figures corresponds to the radial distance from the center of the droplet.

distributions), resulting in generally higher r values at the center, and relatively low values at the periphery ($r_{\text{average}} = 0.97$). Another alternative for changing the deposition patterns was by reducing the overall evaporation rate at the surface of the droplet by slowly drying it in a higher humidity environment (41). This resulted in a larger ring structure for the 1% w/w TRE solution, smoothing the TRE and LYS gradients. However, accumulation of LYS at the outer periphery could not be eliminated (Fig. 9 *a*). At higher TRE concentrations (for the 2.5% w/w and 5% w/w TRE solutions), parabolic distributions for TRE and LYS were observed (Fig. 9, *b* and *c*). Elimination of the variation in the TRE/LYS ratio within the droplet, together with a relatively smaller population of LYS accumulating at the outer periphery, resulted not only in higher r_{average} values, but also higher r values at the outer periphery (Fig. 9, *b* and *c*). These experiments further showed the beneficial effects of eliminating LYS accumulation at the outer periphery.

Initial volume of the droplet (examined by changing the initial solution volume between 0.1 and 10 μl) did not significantly alter the distribution of LYS or TRE (Fig. 10). Due to a smaller aperture size (50 μm $\times$ 50 μm) used for the FTIR analysis of the 0.1 μl droplets, the spectra were noisy, giving unreliable r values. However, the TRE/LYS ratio distributions within the droplets, with $V_i = 0.1$, 1, and 10 μl, were similar (Fig. 10). Only at the very edge of the outer periphery r values dropped to slightly lower values in the $V_i = 1.0$ μl droplet as compared to the $V_i = 10$ μl droplet. This is attributed to the increase in the periphery/volume ratio in the small droplets, which increased the surface area accessible to LYS, and could be a much more significant factor in aerosol or spray drying applications (70).

DISCUSSION

These results showed that not only the chemical composition of the biopreservation solution but also factors, such as non-uniform surface evaporation flux, Marangoni instability, and solute-interface interactions, create spatial heterogeneity and phase separation in drying sessile droplets. These factors caused almost every protein molecule within the same solution to be exposed to different drying and final micro-environmental conditions, making it almost impossible to compare the state(s) of the preserved protein in different solutions or to determine the preservation efficiency of a particular chemical or a biopreservation solution.

The main result of heterogeneity in all of the experimental conditions tested was the variation in the local concentra-

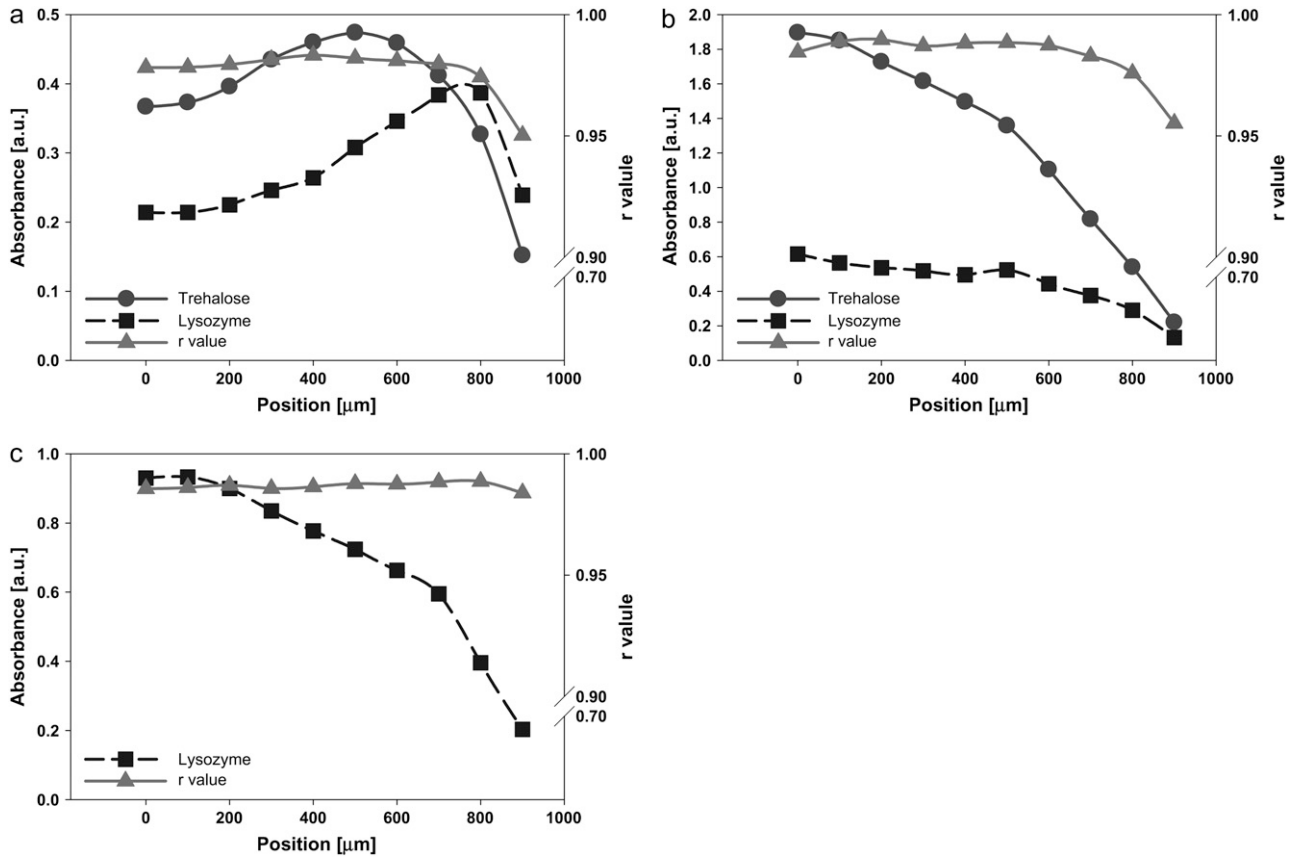

FIGURE 9 Distribution of LYS and TRE and variation of r values within dried (*a*) LYS-TRE (1.0% TRE), (*b*) LYS-TRE (2.5% TRE), and (*c*) LYS-TRE (5% TRE) droplets. The droplets were dried at high humidity. *X* axis (position) in the figures corresponds to the radial distance from the center of the droplet.

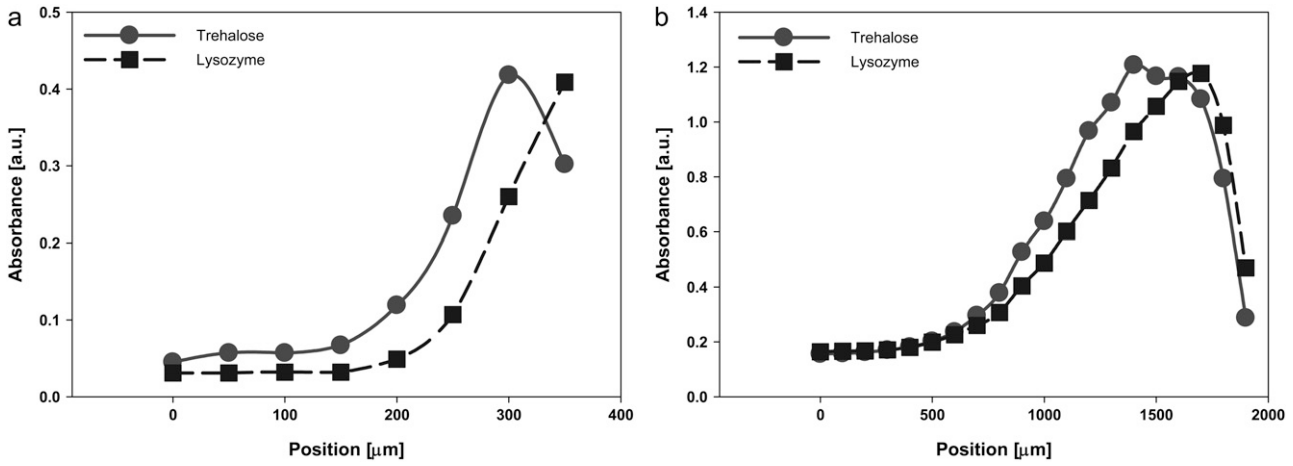

FIGURE 10 Distribution of LYS and TRE within dried (*a*) 0.1 μl and (*b*) 10 μl LYS-TRE (1.0% TRE) droplets. *X* axis (position) in the figures corresponds to the radial distance from the center of the droplet.

tions of TRE (the biopreservation agent) with respect to LYS (the protein to be preserved). This caused the coexistence of different thermodynamic states within the same region in the droplet. Even though the presence of salts in the solution did not directly affect the distribution of the TRE/LYS ratio within the dried droplet (for the concentrations experimented here), it directly affected the structure of LYS. This pointed to a synergistic effect of salts with TRE to stabilize the structure of LYS in a native-like state.

As summarized in Fig. 6, heterogeneous distribution of the solutes determines the accumulation patterns and the secondary structures of the LYS populations within the desiccated droplet. Even though in the initial solution there was enough TRE present to stabilize LYS (49), upon drying LYS separated from TRE, leading to local variations in LYS structure. Note the drop in the *r* values, especially in the outer periphery region for a significant LYS population (40%) in the TRE-LYS samples. This drop is likely to be related to the drop in the TRE/LYS ratio at the outer periphery, as well as the interface-induced denaturation of LYS (71). Variation in the structure of the protein within the droplet was in line with the variation of the amount of residual water, which closely followed the TRE distribution. This was a direct indication of the effect of TRE-water interactions on the secondary structure of LYS.

Separation of LYS from TRE in the outer periphery of the TRE-LYS solutions was one of the most compelling observations in this research. This behavior, at the first look, could be attributed to the well-documented surface affinity of LYS (72). The adsorption kinetics of proteins at the air-liquid interface is affected by the specific sugar type and concentration (73). For globular proteins such as bovine serum albumin (BSA), it is known that surface adsorption of the protein increases with its concentration in the bulk and with the increased bulk concentration of sugars in the ternary solution (74). An opposite behavior is shown for TRE-LYS solutions (75). The timescales associated with the adsorption of BSA and LYS at the surfaces are extremely long (~10–100 min) when compared to the drying timescales observed in this research (~1 min). Besides, the interface adsorption kinetics of LYS is complex, with an initial transient regime when LYS actually migrates away from the liquid-air interface (76). Additionally, the higher viscosity of the solution (due to the addition of TRE and salts), initially and during drying, should be expected to decrease the diffusion of LYS to the surface. The reasons for the observed LYS-TRE separation at the outer periphery could be:

a. The increase in the surface tension with the addition of TRE and the salts (especially LiCl, which increases the surface tension by ~30% in its saturation range) and the resultant increase in the surface affinity of LYS.
b. Increased hydrophobic attractive forces induced by the denaturation of LYS at the interface (71,76), as evidenced by the decreased *r* values at the outer periphery. These hydrophobic forces would then induce aggregation of multiple layers of LYS at the interface. The aggregation of LYS might also alter the behavior of small solids, which accumulate at the edge of the droplet forming a pinned-contact line (41).
c. Tertiary flows induced by local Marangoni instability, which forces LYS to selectively accumulate at the outer periphery. Whatever the mechanism(s) may be, the outcome is the drastic decrease in the TRE/LYS ratio at the outer periphery, causing a steep reduction in *r* values, where most of the LYS population accumulates. This has direct implications in biopreservation research: to reliably determine the preservation efficiency of a particular chemical or solution, or the state of the preserved biological material or organism, it is crucial to analyze the heterogeneities caused by the particular preservation method applied (drying, freezing, or

freeze-drying), and to devise ways to minimize heterogeneity.

Heterogeneity and phase separation were also observed in the LYS-salt droplets, with salt mainly precipitating at the center of the desiccated droplet. This was also observed, although to a lesser extent, in the TRE-LYS-salt samples. The addition of salts to LYS or TRE-LYS solutions slightly increased the amount of LYS accumulated at the periphery. This may be attributed to an increase in the protein-protein interactions and aggregation due to the addition of salts (i.e., salting-out) (77). Accumulation of salts in the form of crystalline hydrates in the center of the droplet, mainly away from the LYS rich periphery, may have more important implications in biopreservation: The only water left in the sample would be associated with the salt crystals, and therefore would be unavailable to LYS. This would yield to erroneous conclusions if the overall water content of the desiccated droplet (which is usually measured by Karl-Fischer titration or differential scanning calorimetry, or thermogravimetrically by simply baking the sample at temperatures $>100°C$) is used to measure the hydration level of the LYS in the droplet, or the availability of water in the sample is used to deduct conclusions about the state of the preserved protein. Building on our observations, we can hypothesize that most, if not all, of the measurements reported in the biopreservation literature that rely on gross measurement methods such as those outlined above must have, to some degree, been affected by the heterogeneity in the samples.

There may be several reasons for the measurement of higher r values in the LYS-$CaCl_2$ and LYS-$MgCl_2$ samples, when compared to LYS-NaCl and LYS-LiCl solutions. One possibility is that there is a greater amount of water in the samples due to the presence of highly charged Ca^{2+} and Mg^{2+} ions. The interaction of the Ca^{2+} or the Mg^{2+} ions with LYS, similar to that described by Arakawa for BSA (50), may also change a part of the LYS structure, causing it to resemble fully hydrated LYS. The third possibility is that salt-associated water (in crystalline-hydrate structures) may be, to some degree, available to the protein.

Our results indicate that the addition of salts helped stabilize the protein structure within the TRE matrix. All salts affected the CH vibrations of TRE (Fig. 7 *b*), which was attributed to the effect of the cations on hydrogen bonding (63), especially since the Cl^- anion is very weak in terms of its water structuring ability (78). NaCl in the presence of TRE had only a marginally beneficial effect on the LYS structure, as it did not have any specific interactions, and crystallized out of the sample (this was observed optically with transmitted light microscopy). The effect of $CaCl_2$ is difficult to determine, as it can interact both with LYS and TRE. However, its strong interactions with TRE are likely to be detrimental for the LYS structure, since TRE and $CaCl_2$, upon drying, can form monohydrate crystals (68). LiCl and $MgCl_2$ in combination with TRE act to stabilize the structure of the protein. As LiCl alone does not stabilize the protein structure, there must be a synergistic effect between the LiCl and TRE, which protects the protein against desiccation. However, in terms of their ability to form complexes with carbohydrates, cations have been ranked by Angyal et al. (55) as $Li^+ < Na^+ < Mg^{2+} < Ca^{2+}$. Hence, it is unlikely that the Li^+ ion had any strong interaction with TRE. One possible explanation for the higher r values in the LYS-TRE-LiCl sample, and also the associated higher glycosidic bond and CH vibration frequencies, is the effect of the Li^+ ion on the residual water. Although the mobility of the water in the first hydration layer of the Li^+ ion is less than in the bulk (78), the water molecules in the secondary and tertiary hydration layers are more mobile. This is also seen, to a lesser extent, in Na^+ ions. The ions affect the residual water (by destructuring) thereby freeing the water molecules to make hydrogen bonds with TRE and LYS. Therefore, it is possible that the destructuring of water increases the probability of the formation of TRE-H_2O-LYS complexes (79), preserving LYS structure. This explanation is also supported by the higher degree of hydrogen bonding in TRE observed by the shift in the ν-OH peaks to lower wavenumbers.

Higher TRE concentrations cause higher degrees of intramolecular hydrogen bonding (80), which should lower the flexibility of the TRE molecules (similar to that seen for sucrose (81)). Higher concentrations of TRE also have a lower glycosidic bond frequency (63). As the glycoside oxygen does not participate in hydrogen bonding (80), it is reasonable to suggest that the lower glycosidic bond frequency corresponds to the lowered flexibility of the TRE molecule. One result of a change in the water organization may therefore be an increased effective hydration and hence reduced intramolecular hydrogen bonding of the TRE molecule, which would increase its flexibility, similar to what was observed by Krischner (82) for $1\rightarrow6$ linked carbohydrates. Hence, residual water probably mediates the interactions among the protein, TRE, and salt (except Ca^{2+}). Due to specific interactions with the Ca^{2+} ion, TRE molecules participate in a TRE-salt complex, and their glycosidic frequency is lowered. Hypotheses are offered that link the flexibility of the TRE molecule to its protective ability (81,83). Additionally, there are reports (79,84) with evidence supporting the hypothesis that water molecules mediate TRE-protein interactions, thereby allowing the sugar matrix to more easily conform to the surface of the protein.

Our results and the discussions above helped us predict that a higher TRE concentration in the biopreservation solution would eliminate the peripheral flow that induces macroheterogeneity by causing selective accumulation of solutes at the periphery and TRE-LYS separation, whereas moderate amounts of LiCl in the solution would help eliminate the microheterogeneity caused by the uneven distribution of the residual water. Experiments were conducted to test this prediction. It was observed for a combination of 5% TRE solution and 1:1 LiCl ratio that uniform r values >0.99 could

be obtained throughout the desiccated droplet (Fig. 11 *a*). As predicted, increasing the LiCl concentration in the solution (to 1:5) reduced the overall *r* values (~0.85) due to specific interactions between the LiCl and protein (Fig. 11 *b*).

In this study, the model protein used was lysozyme due to the fact that its properties and behavior have been characterized in detail in the literature, and that there are reports establishing its interactions with salts and trehalose. One of the drawbacks of using lysozyme as the model protein is that it is very resistant to thermal, osmotic, and chemical denaturation. For example, excessive dehydration of LYS under vacuum for several hours did not lower $r_{average}$ below 0.68. As such, the synergistic effects of LiCl with TRE reported here may even be underestimated. Since the purpose of this study was to highlight the effects of heterogeneity and specific interactions of cosolutes on the protein structure during preservation, this is not considered to be a major handicap. However, it warrants future studies with more susceptible proteins. As previously mentioned in the Introduction, the structure of the protein during preservation is directly related to its poststorage function and activity. To determine the poststorage function and to establish its correlation with the protein secondary structure during preservation, postdesiccation activity experiments were also conducted, which showed that the proteins desiccated in TRE-LYS-LiCl and TRE-LYS-$MgCl_2$ solutions indeed had the highest poststorage activity (E. Reategui, V. Ragoonanan, and A. Aksan, unpublished data).

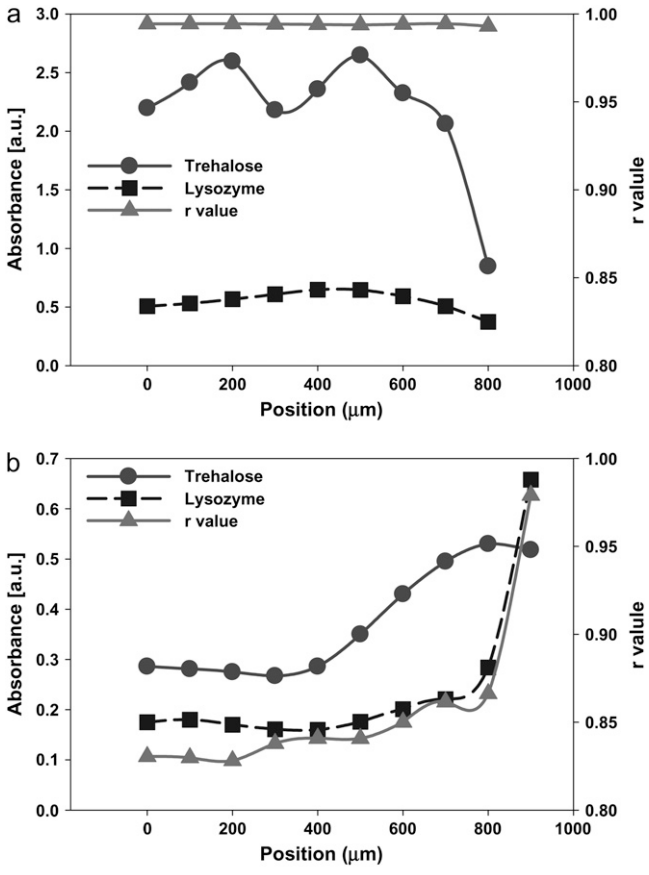

FIGURE 11 Distribution of LYS and TRE and variation of *r* values within dried (*a*) LYS-TRE-LiCl (5% TRE; 1:1 LiCl) and (*b*) LYS-TRE-LiCl (1% TRE; 1:5 LiCl) droplets. *X* axis (position) in the figures corresponds to the radial distance from the center of the droplet.

The driving potential behind the peripheral flow is the evaporation rate flux difference between the center of the droplet (J''_C), and the edge (J''_E), which is expressed as $\Delta J'' = J''_C - J''_E$. If D is the diffusivity and R (radius) is the characteristic length of the droplet, then the flow stress exerted on the solutes can be expressed as $D \times \Delta J''/R$. On the other hand, the viscous drag force on the solutes is $\mu \times v \times R$, where μ is the viscosity of the solution and v is the characteristic speed of the peripheral flow. The viscous drag stress is then $\mu \times v/R$. The flow condition is determined by the tug-of-war between these two stresses. Therefore, the characteristic flow speed is scaled as $v \sim \Delta J'' \times D/\mu$. The Stokes-Einstein relationship establishes an inverse relationship between diffusivity and viscosity at constant temperature. Therefore, the characteristic speed of the flow scales as $v \sim \Delta J''/\mu^2$. With $\Delta J'' \sim O(-3)$ (85), and $\mu \sim O(-4)$ reasonable values for the characteristic speed on the order of μm/s is predicted. This scaling law implies that a change in the viscosity of the solution would have a strong effect (inverse squared) on the flow speed and can potentially stop it for all practical purposes. This explains the cessation of flow in the sessile droplets when the TRE concentration is increased from 1% to 5% (with an increase of ~40% in viscosity), which results in halving of the characteristic flow speed. The fact that characteristic flow speed is not a function of R also supports our observations that the droplet size does not have a significant effect on the flow or deposition patterns. The peripheral flow could also be stopped by increasing the RH of the surrounding air. This indicates that not only the difference but also the magnitude of the evaporation flux is a factor determining the flow conditions. As discussed before, the Marangoni instability is a function of the variation of the surface tension, σ, with concentration, c, and temperature T. Therefore, a future full analysis of the flow condition should be based on a functional such as: $v = f(\Delta J'', J''_E, D, \mu, \partial\sigma/\partial c, \partial\sigma/\partial T)$.

CONCLUSIONS

Currently, to our knowledge, there are no published studies exploring the role of spatial heterogeneity induced during preservation processes (cryopreservation, desiccation, or lyophilization) on the viability and function of preserved biomolecules and biological systems. In this manuscript, we focused on the interactions of proteins with widely used stabilizers and explored the physical and chemical mechanisms of heterogeneity induced during isothermal desiccation of sessile droplets. We conclude that:

1. Peripheral flow, caused by contact line pinning and nonuniform surface evaporation flux, is the dominant

flow within drying droplets, causing 40–70% of the solutes to accumulate at the outer periphery in the form of a ring.

2. During drying of sessile droplets, separation of its constituents is the major source of heterogeneity. In this study, the separation of LYS from TRE causing a lower TRE/LYS ratio at the outer periphery was identified as the major reason for the LYS structural modification at the outer periphery. The presence of sugars (such as trehalose) at high concentrations in the biopreservation solution slows the peripheral flow, reducing the main driving force behind separation.
3. Separation of constituents is also aggravated by specific interactions of proteins with interfaces. This can be minimized by changing the drying conditions (slower drying rates and establishing a more uniform surface evaporation flux), increasing the concentrations of sugars in the solution to increase viscosity, and by adding salts to alter the surface affinity of proteins.
4. The secondary flow instability in desiccating droplets is the Marangoni instability that may result in specific accumulation of solutes in certain regions. The force or the onset conditions of the Marangoni flow can be controlled by changing the drying conditions and by the addition of salts to the preservation solution. The presence of salts in the solution disrupts the Marangoni flow in LYS-salt solutions and enhances the accumulation of LYS at the edge of the droplet in LYS-TRE-salt solutions.
5. Upon drying, the secondary structure of lysozyme changes from its native state. The overall change is minimal in the presence of salts and trehalose, followed by trehalose only. Small spatial variations in the lysozyme structure within the dried droplet are induced by the variations in the local concentrations of salts and trehalose with respect to lysozyme.
6. Formation of crystalline hydrates in the dried solution, or entrapment of water in the trehalose matrix, may cause overestimation of the water available to the protein in the desiccated product. This may result in overestimation of the water content or its availability to the protein.
7. At low concentrations, LiCl acts synergistically with trehalose to preserve the native structure of lysozyme in the dried state. The mechanism is attributed to the effect of the Li^+ on the structure of the residual water. However, at high concentrations it causes significant reduction in r values due to protein-salt interactions. Salts destructure the residual water (excluding the first couple of hydration layers), which in turn alters the hydrogen bonded network. The water molecules in these layers are then more free to mediate interactions between the protein and trehalose (this was first observed by Cottone (79)). The effect of the destructured water and its subsequent ability to mediate protein-trehalose interactions are seen in the CH vibrations, and the glycosidic flexibility of the trehalose molecule and the higher r values measured in the LYS-TRE-LiCl samples. Therefore, the main effect of the salts is through the modification of the flexibility of the trehalose molecule, increasing its protective capabilities.

SUMMARY

We have explored the mechanisms of heterogeneity in desiccated sessile droplets of trehalose-salt solutions containing lysozyme. We have utilized FTIR spectroscopy to quantify heterogeneity in the deposition patterns of the respective constituents in the solution as well as the effect of this on the structure of trehalose and the protein. We have observed separation of the protein from trehalose, especially in the outer periphery of the droplet at low sugar concentrations. This was mainly caused by the dominant peripheral flow induced in the droplet. A progressively more uniform protein accumulation at the center of the droplet could be achieved by increasing the trehalose concentration in the solution, adding specific salts, and controlling the evaporation flux gradients at the droplet surface (41). A direct link has been shown to exist between trehalose structure and its ''protection efficiency'', and protein distribution and its structure. Studies are under way to quantify the effects of freezing and freeze-drying-induced heterogeneities on the poststorage activity and viability of proteins, bacteria, and mammalian cells.

The authors thank Dr. Wim Wolkers for careful reading of the manuscript and his suggestions. We also thank the anonymous reviewers for their thoughtful comments and suggestions.

This research is supported by a grant (GIA-20328) from the Office of the Dean of the Graduate School of the University of Minnesota.

REFERENCES

1. Prestrelski, S. J., N. Tedeschi, T. Arakawa, and J. F. Carpenter. 1993. Dehydration-induced conformational transitions in proteins and their inhibition by stabilizers. *Biophys. J.* 65:661–671.
2. Frauenfelder, H., P. W. Fenimore, G. Chen, and B. H. McMahon. 2006. Protein folding is slaved to solvent motions. *Proc. Natl. Acad. Sci. USA.* 103:15469–15472. doi:10.1073/pnas.0607168103
3. Gekko, K., and T. Morikawa. 1981. Thermodynamics of polyol-induced thermal stabilization of chymotrypsinogen. *J. Biochem.* (*Tokyo*). 90:51–60.
4. Perez, C., P. De Jesus, and K. Griebenow. 2002. Preservation of lysozyme structure and function upon encapsulation and release from poly (lactic-co-glycolic) acid microspheres prepared by the water-in-oil-in-water method. *Int. J. Pharm.* 248:193–206. doi:10.1016/S0378-5173(02)00435-0
5. Allison, S. D., B. S. Chang, T. W. Randolph, and J. F. Carpenter. 1999. Hydrogen bonding between sugar and protein is responsible for inhibition of dehydration-induced protein folding. *Arch. Biochem. Biophys.* 223:289–298. doi:10.1006/abbi.1999.1175
6. Choi, J. H. and J. C. Bischof. 2008. A quantitative analysis on the thermal properties of phosphate buffered saline with glycerol at subzero temperatures. International Journal of Heat and Mass Transfer. 51:640–649.

7. Izutsu, K., S. Yoshioka, S. Kojima, T. W. Randolph, and J. F. Carpenter. 1996. Effects of sugars and polymers on crystallization of poly(ethylene glycol) in frozen solutions: phase separation between incompatible polymers. *Pharm. Res.* 17:1316–1322. doi:10.1023/A:1026412107574
8. Izutsu, K., M. C. Heller, T. W. Randolph, and J. F. Carpenter. 1998. Effects of salts and sugars on phase separation of polyvinylpyrrolidone-dextran solutions induced by freeze-concentration. *J. Chem. Soc., Faraday Trans.* 84:411–417. doi:10.1039/a704950a
9. Izutsu, K., and S. Kojima. 2000. Freeze-concentration separates proteins and polymer excipients into different amorphous phases. *Pharm. Res.* 17:1316–1322. doi:10.1023/A:1026412107574
10. Strambini, G. B., and M. Gonnelli. 2007. Protein stability in ice. *Biophys. J.* 92:2131–2138. doi:10.1529/biophysj.106.099531
11. Rabin, Y., P. S. Steif, K. C. Hess, J. L. Jimenez-Rios, and M. C. Palastro. 2006. Fracture formation in vitrified thin films of cryoprotectants. *Cryobiology.* 53:75–95.
12. Aksan, A., S. C. Morris, and M. Toner. 2005. Analysis of desiccation and vitrification characteristics of carbohydrate films by shear wave resonators. *Langmuir.* 21:2847–2854. doi:10.1021/la047760y
13. Aksan, A., D. Irimia, X. He, and M. Toner. 2006. Desiccation kinetics of biopreservation solutions in microchannels. *J. Appl. Phys.* 99: 064703. doi:10.1063/1.2181280
14. Heller, M. C., J. F. Carpenter, and T. W. Randolph. 1999. Protein formulation and lyophilization cycle design: prevention of damage due to freeze-concentration induced phase separation. *Biotechnol. Bioeng.* 63:166–174. doi:10.1002/(SICI)1097-0290(19990420)63:2⟨166::AID-BIT5⟩3.0.CO;2-H
15. Suzuki, T., and F. Franks. 1993. Solid-liquid phase transitions and amorphous states in ternary sucrose-glycine-water systems. *J. Chem. Soc., Faraday Trans.* 89:3283–3288. doi:10.1039/ft9938903283
16. Shalaev, E. Y., and A. N. Kanev. 1994. Study of the solid-liquid state diagram of the water-glycine-sucrose system. *Cryobiology.* 31:374–382. doi:10.1006/cryo.1994.1045
17. Shalaev, E. Y., and F. Franks. 1996. Changes in the physical state of model mixtures during freezing and drying: impact on product quality. *Cryobiology.* 33:11–26. doi:10.1006/cryo.1996.0002
18. Murase, N., and F. Franks. 1989. Salt precipitation during the freeze-concentration of phosphate buffer solutions. *Biophys. Chem.* 34:293–300. doi:10.1016/0301-4622(89)80066-3
19. Randolph, T.W. 1997. Phase Separation of Excipients during Lyophilization: Effects on Protein Stability. *J. Pharm. Sci.* 86:1198–1203.
20. Heller, M. C., J. F. Carpenter, and T. W. Randolph. 1999. Application of a thermodynamic model to the prediction of phase separations in freeze-concentrated formulations for protein lyophilization. *Arch. Biochem. Biophys.* 363:191–201. doi:10.1006/abbi.1998.1078
21. Jovanovic, N., A. Gerich, A. Bouchard, and W. Jiskoot. 2006. Near-infrared imaging for studying homogeneity of protein-sugar mixtures. *Pharm. Res.* 23:2002–2013. doi:10.1007/s11095-006-9037-y
22. Murase, N., P. Echlin, and F. Franks. 1991. The structural states of freeze-concentrated and freeze-dried phosphates studied by scanning electron microscopy and differential scanning calorimetry. *Cryobiology.* 28:364–375. doi:10.1016/0011-2240(91)90043-N
23. Heller, M. C., J. F. Carpenter, and T. W. Randolph. 1997. Manipulation of lyophilization-induced phase separation: implications for pharmaceutical proteins. *Biotechnol. Prog.* 13:590–596. doi:10.1021/bp970081b
24. Heller, M. C., J. F. Carpenter, and T. W. Randolph. 1996. Effects of phase separating systems on lyophilized hemoglobin. *J. Pharm. Sci.* 85:1358–1362. doi:10.1021/js960019t
25. Carpenter, J. F., and B. S. Chang. 1996. Lyophilization of protein pharmaceuticals. *In* Biotechnology and Biopharmaceutical Manufacturing, Processing and Preservation. K. Avis and V. Wu, editors. Intep0harm Press, Buffalo Grove. 199–264.
26. Rey, L., and J. C. May, editors. 1999. Freeze-Drying/Lyophilization of Pharmaceutical and Biological Products. Marcel Dekker, New York.
27. Webb, S. J. 1965. Bound Water in Biological Activity. Charles C. Thomas, Springfield, IL.
28. Suihko, E. J., R. T. Forbes, and D. C. Apperley. 2005. A solid-state NMR study of molecular mobility and phase separation in co-spray-dried protein-sugar particles. *Eur. J. Pharm. Sci.* 25:105–112. doi:10.1016/j.ejps.2005.02.002
29. Norris, M. M., A. Aksan, K. Sugimachi, and M. Toner. 2006. 3-O-methyl-D-glucose improves desiccation tolerance of keratinocytes. *Tissue Eng.* 12:1–7. doi:10.1089/ten.2006.12.1873
30. Bhowmick, S., L. Zhu, L. K. McGinnis, J. A. Lawitts, B. D. Nath, M. Toner, and J. D. Biggers. 2003. Desiccation tolerance of spermatozoa at ambient temperature: production of fetal mice. *Biol. Reprod.* 68:1779–1786. doi:10.1095/biolreprod.102.009407
31. de Gans, B.-J., and U. S. Schubert. 2004. Inkjet printing of well-defined polymer dots and arrays. *Langmuir.* 20:7789–7793. doi:10.1021/la049469o
32. Flickinger, M. C., J. L. Schottel, D. R. Bond, A. Aksan, and L. E. Scriven. 2007. Painting and printing living bacteria: engineering nanoporous biocatalytic coatings to preserve microbial viability and intensify reactivity. *Biotechnol. Prog.* 23:2–17. doi:10.1021/bp060347r
33. Park, J., and J. Moon. 2006. Control of colloidal particle deposition patterns within picoliter droplets ejected by ink-jet printing. *Langmuir.* 22:3506–3513. doi:10.1021/la053450j
34. Dugas, V., J. Broutin, and E. Souteyrand. 2005. Droplet evaporation study applied to DNA chip manufacturing. *Langmuir.* 21:9130–9136. doi:10.1021/la050764y
35. Blossey, R., and A. Bosio. 2002. Contact line deposits on cDNA microarrays: A ''twin spot effect''. *Langmuir.* 18:2952–2954. doi:10.1021/la0114732
36. Tarasevich, Y. Y., and D. M. Pravoslavnova. 2007. Segregation in desiccated sessile drops of biological fluids. *Eur. Phys. J. E.* 22:311–314. doi:10.1140/epje/e2007-00037-6
37. Filik, J., and N. Stone. 2007. Drop coating deposition Raman spectroscopy of protein mixtures. *Analyst.* 132:544–550. doi:10.1039/b701541k
38. Zhang, D., Y. Xie, M. F. Mrozek, C. Ortiz, V. J. Davisson, and D. Ben-Amotz. 2003. Raman detection of proteomic analytes. *Anal. Chem.* 75:5703–5709. doi:10.1021/ac0345087
39. Sommer, A. P., M. Ben-Moshe, and S. Magdassi. 2004. Size-discriminative self-assembly of nanospheres in evaporating drops. *J. Phys. Chem. B.* 108: 8–10. doi:10.1021/jp0363747
40. Li, Q., Y. T. Zhu, I. A. Kinloch, and A. H. Windle. 2006. Self-organization of carbon nanotubes in evaporating droplets. *J. Phys. Chem. B.* 110:13926–13930. doi:10.1021/jp061554c
41. Deegan, R. D., O. Bakajin, T. F. Dupont, G. Huber, S. R. Nagel, and T. A. Witten. 2000. Contact line deposits in an evaporating drop. *Phys. Rev. E Stat. Phys. Plasmas Fluids Relat. Interdiscip. Topics.* 62:756–765.
42. Caddock, B. D., and D. Hull. 2002. Influence of humidity on the cracking patterns formed during the drying of sol-gel drops. *J. Mater. Sci.* 37:825–834. doi:10.1023/A:1013808402289
43. Hu, H., and R. G. Larson. 2006. Marangoni effect reverses coffee-ring depositions. *J. Phys. Chem. B.* 110:7090–7094. doi:10.1021/jp0609232
44. Ha, V.-M., and C.-L. Lai. 2002. Onset of Marangoni instability of a two-component evaporating droplet. *International Journal of Heat and Mass Transfer.* 45:5143–5158. doi:10.1016/S0017-9310(02)00222-3
45. Kaminskii, V. A., and V. V. Dil'man. 2003. Marangoni instability in evaporation of binary mixtures. *Theor. Found. Chem. Eng.* 37:533–538. doi:10.1023/B:TFCE.0000007898.04154.5f
46. Hu, H., and R. G. Larson. 2005. Analysis of the microfluidic flow in an evaporating sessile droplet. *Langmuir.* 21:3963–3971. doi:10.1021/la047528s
47. Kaushik, J. K., and R. Bhat. 2003. Why is trehalose an exceptional protein stabilizer? *J. Biol. Chem.* 278:26458–26465. doi:10.1074/jbc.M300815200
48. Crowe, J. H., L. M. Crowe, and D. Chapman. 1984. Preservation of membranes in anhydrobiotic organisms—the role of trehalose. *Science.* 223:701–703. doi:10.1126/science.223.4637.701

49. Carpenter, J. F., and J. H. Crowe. 1989. An infrared spectroscopic study of the interactions of carbohydrates with dried proteins. *Biochemistry*. 28:3916–3922. doi:10.1021/bi00435a044

50. Arakawa, T., and S. N. Timasheff. 1982. Preferential interactions of proteins with salts in concentrated solutions. *Biochemistry*. 21:6545–6552. doi:10.1021/bi00268a034

51. Broering, J. M., and A. S. Bommarius. 2005. Evaluation of Hofmesiter effects on the kinetic stability of proteins. *J. Phys. Chem. B*. 109: 20612–20619. doi:10.1021/jp053618+

52. Mazzobre, M. F., and M. D. Buera. 1999. Combined effects of trehalose and cations on the thermal resistance of β-galactosidase in freeze-dried systems. *Biochimica Et Biophysica Acta (BBA)-General Subjects*. 1473:337–344. doi:10.1016/S0304-4165(99)00207-X

53. Carpenter, J. F., S. C. Hand, L. M. Crowe, and J. H. Crowe. 1986. Cryoprotection of phosphofructokinase with organic solutes—characterization of enhanced protection in the presence of divalent-cations. *Arch. Biochem. Biophys.* 250:505–512. doi:10.1016/0003-9861(86)90755-1

54. Alekseev, Y. E., A. D. Garnovskii, and Y. A. Zhdanov. 1998. Complexes of natural carbohydrates with metal cations. *Russ. Chem. Rev*. 67:649–669. doi:10.1070/RC1998v067n08ABEH000343

55. Angyal, S. J. 1989. Complexes of metal cations with carbohydrates in solution. *Adv. Carbohydr. Chem. Biochem*. 47:1–43.

56. Miller, D. P., J. J. de Pablo, and H. R. Corti. 1999. Viscosity and glass transition temperature of aqueous mixtures of trehalose with borax and sodium chloride. *J. Phys. Chem. B*. 103:10243–10249. doi:10.1021/jp984736i

57. Timasheff, S. N. 2002. Protein hydration, thermodynamic binding, and preferential hydration. *Biochemistry*. 41:13473–13482. doi:10.1021/bi020316e

58. McGinnis, L. K., L. Zhu, J. A. Lawitts, S. Bhowmick, M. Toner, and J. D. Biggers. 2005. Mouse sperm desiccated and stored in trehalose medium without freezing. *Biol. Reprod.* 73:627–633. doi:10.1095/biolreprod.105.042291

59. Chen, T., J. P. Acker, A. Eroglu, S. Cheley, H. Bayley, A. Fowler, and M. L. Toner. 2001. Beneficial effect of intracellular trehalose on the membrane integrity of dried mammalian cells. *Cryobiology*. 43:168–181. doi:10.1006/cryo.2001.2360

60. Alvarez, J., D. C. Lee, S. A. Baldwin, and D. Chapman. 1987. Fourier transform infrared spectroscopic study of the structure and conformational changes of the human erythrocyte glucose transporter. *J. Biol. Chem.* 262:3502–3509.

61. Nyquist, R. A., C. L. Putzig, and M. A. Leugers. 1997. The Handbook of Infrared and Raman Spectra of Inorganic Compounds and Organic Salts, Vol. 4. Academic Press, San Diego.

62. Adams, L. H., and R. E. Gibson. 1930. The melting curve of sodium chloride dihydrate. An experimental study of an incongruent melting at pressures up to twelve thousand atmospheres. *J. Am. Chem. Soc.* 52:4252–4264. doi:10.1021/ja01374a010

63. Kačuráková, M., and M. Mathlouthi. 1996. FTIR and laser-Raman spectra of oligosaccharides in water: characterization of the glycosidic bond. *Carbohydr. Res.* 284:145–157. doi:10.1016/0008-6215(95)00412-2

64. Careri, G., and A. Giansanti. 1979. Lysozyme film hydration events: an IR gravimetric study. *Biopolymers*. 18:1187–1203. doi:10.1002/bip.1979.360180512

65. Mizughchi, M. 1997. Fourier-transform infrared spectroscopic studies on the coordination of the side-chain COO-groups to Ca^{2+} in equine lysozyme. *Eur. J. Biochem.* 250:72–76. doi:10.1111/j.1432-1033.1997.00072.x

66. van Stokkum, I. H. M., H. Linsdell, J. M. Hadden, P. I. Haris, D. Chapman, and M. Bloemendal. 1995. Temperature-induced changes in protein structures studied by Fourier transform infrared spectroscopy and global analysis. *Biochemistry*. 34:10508–10518. doi:10.1021/bi00033a024

67. Oku, K., M. Kurose, M. Kubota, S. Fukuda, M. Kurimoto, Y. Tujisaka, and M. Sakurai. 2005. Interaction between trehalose and alkaline-earth metal ions. *Biosci. Biotechnol. Biochem.* 69:7–12. doi:10.1271/bbb.69.7

68. Fujimoto, T., K. Oku, M. Tashiro, and T. Machinami. 2006. Crystal structure of α, α-trehalose–calcium chloride monohydrate complex. *J. Carbohydr. Chem.* 25:521–532. doi:10.1080/07328300600966414

69. Wolkers, W. F., A. E. Oliver, F. Tablin, and J. H. Crowe. 2004. A Fourier-transform infrared spectroscopy study of sugar glasses. *Carbohydr. Res.* 339:1077–1085.

70. Adler, M., and G. Lee. 1999. Stability and surface activity of lactate dehydrogenase in spray-dried trehalose. *J. Pharm. Sci*. 88:199–208. doi:10.1021/js980321x

71. Lu, J. R., T. J. Su, R. K. Thomas, J. Penfold, and J. Webster. 1998. Structural conformation of lysozyme layers at the air/water interface studied by neutron reflection. *J. Chem. Soc., Faraday Trans.* 94:3279–3287. doi:10.1039/a805731a

72. Hunter, J. R., P. K. Kilpatrick, and R. G. Carbonell. 1990. Lysozyme adsorption at the air/water interface. *J. Colloid Interface Sci*. 137:462–482. doi:10.1016/0021-9797(90)90421-J

73. Guzey, D., D. J. McClements, and J. Weiss. 2003. Adsorption kinetics of BSA at air-sugar solution interfaces as affected by sugar type an concentration. *Food Res. Int.* 36:649–660. doi:10.1016/S0963-9969(03)00004-8

74. Rodrigez Nino, M. R., and J. M. Rodrigez Patino. 2002. Effect of the aqueous phase composition on the adsorption of bovine serum albumin to the air-water interface. *Ind. Eng. Chem. Res*. 41:1489–1495. doi:10.1021/ie010770z

75. Wendorf, J. R., C. J. Radke, and H. W. Blanch. 2004. Reduced protein adsorption at solid interfaces by sugar excipients. *Biotechnol. Bioeng*. 87:565–573. doi:10.1002/bit.20132

76. Xu, S., and S. Damodaran. 1992. The role of chemical potential in the adsorption of lysozyme at the air-water interface. *Langmuir*. 8:2021–2027. doi:10.1021/la00044a024

77. Curtis, R. A., J. Ulrich, A. Montaser, J. M. Prausnitz, and H. W. Blanch. 2002. Protein-protein interactions in concentrated electrolyte solutions. *Biotechnol. Bioeng*. 79:367–380. doi:10.1002/bit.10342

78. Collins, K. D. 1995. Sticky ions in biological-systems. *Proc. Natl. Acad. Sci. USA*. 92:5553–5557. doi:10.1073/pnas.92.12.5553

79. Cottone, G., G. Ciccotti, and L. Cordone. 2002. Protein–trehalose–water structures in trehalose coated carboxy-myoglobin. *J. Chem. Phys*. 117: 9862–9866. doi:10.1063/1.1518960

80. Conrad, P. B., and J. J. de Pablo. 1999. Computer simulation of cryoprotectant disaccharide α,α-trehalose in aqueous solution. *J. Phys. Chem. A*. 103:4049–4055. doi:10.1021/jp984102b

81. Lerbret, A., P. Bordat, F. Affouard, M. Descamps, and F. Migliardo. 2005. How homogeneous are the trehalose, maltose, and sucrose water solutions? An Insight from molecular dynamics simulations. *J. Phys. Chem. B*. 109:11046–11057. doi:10.1021/jp0468657

82. Kirschner, K. N., and R. J. Woods. 2001. Solvent interactions determine carbohydrate conformation. *Proc. Natl. Acad. Sci. USA*. 98:10541–10545. doi:10.1073/pnas.191362798

83. Magazu, S., G. Maisano, P. Migliardo, A. M. Musolino, and V. Villari. 1998. Fragile-like behaviour and H-bond interactions of the glass-forming water-trehalose system. *Philosophical Magazine*. 77:655–661.

84. Cordone, L., G. Cottone, S. Giuffrida, G. Palazzo, G. Venturoli, and C. Viappiani. 2005. Internal dynamics and protein-matrix coupling in trehalose-coated proteins. *Biochimica Et Biophysica Acta (BBA)-Proteins and Proteomics*. 1749:252–281. doi:10.1016/j.bbapap.2005.03.004

85. Widjaja, E., N. C. Liu, M. Li, R. T. Collins, O. A. Basaran, and M. T. Harris. 2007. Dynamics of sessile droplet evaporation: a comparison of the spine and the elliptic mesh generation methods. *Comput. Chem. Eng*. 31:219–232.